Eur. Phys. J. B **14**, 627–632 (2000)

THE EUROPEAN PHYSICAL JOURNAL B

EDP Sciences

Phase transitions in $Sr_{0.61}Ba_{0.39}Nb_2O_6$:$Ce^{3+}$: I. Susceptibility of clusters and domains

J. Dec[1,a], W. Kleemann[1,b], Th. Woike[2], and R. Pankrath[3]

[1] Laboratorium für Angewandte Physik, Gerhard Mercator-Universität, 47048 Duisburg, Germany
[2] Institut für Kristallographie, Zülpicher Straße 49b, Universität zu Köln, 50674 Köln, Germany
[3] Fachbereich Physik, Universität Osnabrück, 49076 Osnabrück, Germany

Received 1 October 1999

Abstract. The complex dielectric susceptibility of $Sr_{0.61}Ba_{0.39}Nb_2O_6$:$Ce^{3+}$ (SBN61:Ce) has been measured at frequencies $10^2 \leq f \leq 10^7$ Hz and temperatures $300 \leq T \leq 470$ K before and after poling. The relaxor behaviour with large polydispersivity observed above the ferroelectric phase transition temperature, $T_c = 360$ and 340 K for $x(\mathrm{Ce}) = 0$ and 0.0066, respectively, is perfectly modeled within the framework of Chamberlin's dynamically correlated domain approach. Below T_c the dynamic nanodomain state crosses over into a ferroelectric state with polydispersive domain wall dynamics at very low frequencies. Presumably SBN61:Ce belongs to the three-dimensional random field Ising rather than to the dipole glass universality class.

PACS. 64.70.Pf Glass transitions – 77.22.Ch Permittivity (dielectric function) – 77.80.-e Ferroelectricity and antiferroelectricity – 77.84.Dy Niobates, titanates, tantalates, PZT ceramics etc.

1 Introduction

Strontium-barium niobate, $Sr_xBa_{1-x}Nb_2O_6$ (SBN for short), is a promising material due to its very attractive pyroelectric [1], piezoelectric [2], electrooptic [3,4], acoustooptic [5], photorefractive [6–9] and non-linear optic [10] properties. Very probably the most spectacular application concerns the reversible optical memory units [11].

SBN belongs to the tetragonal tungsten bronze ferroelectric oxide family of the general formula AB_2O_6. The congruently melting $Sr_{0.61}Ba_{0.39}Nb_2O_6$ (SBN61) composition is a bronze with small unit cell and tetragonal 4mm crystal structure at room temperature as determined by X-ray diffraction investigations [12]. This double solid solution system may be represented by the structural formula $A'_2A''_4C_4B'_2B''_8O_{30}$ which takes into account the total number of different sites and non-equivalency of the oxygen octahedra [13]. The twelve-fold (A′) coordinated sites are occupied only by the smaller Sr^{2+} (ionic radius $r = 1.12$ Å) ions, the fifteen-fold (A″) – both by the Sr^{2+} and the larger Ba^{2+} ($r = 1.34$ Å) ions, whereas the smallest nine-fold coordinated vacancies are empty. Since only 5/6 of the A sites are occupied, SBN61 is referred to as an unfilled bronze [12] and the vacancies of the other 1/6 A sites act as carrier trapping centers [14]. Thus the ferroelectric unit cell contains five formal AB_2O_6 units. The high-temperature prototype symmetry is tetragonal 4/mmm, placing SBN61 into the Shuvalov ferroelectric species 4/mmm(1)D4F4mm [15]. In the ferroelectric phase all the metallic ions are shifted along the tetragonal polar axis. At the transition into the paraelectric phase the Ba^{2+} and Sr^{2+} as well as 20% of Nb^{5+} (B′) ions move towards symmetrical positions in the oxygen planes, whereas the rest of 80% of Nb^{5+} (B″) ions are equivalently distributed above and below the oxygen layers (Ref. [13], p. 106).

In contrast with the pure SBN61 system the doped ones are of practical importance. It is well-known that dopants enhance various physical properties. In particular, SBN61 doped with rare-earth metal ions are most efficient photorefractive materials widely used for holographic applications [16]. These dopants are strongly lowering the phase transition temperature, T_c, of SBN61 thus allowing to control many of the ferroelectric properties [16,17]. Non-equivalent substitutions and the unfilled type of structure of SBN favor the formation of local, randomly up or down oriented polar regions even far above T_c. Evidence of such precursor phenomena in pure SBN has already been obtained from specific-heat [18], Raman [19] second-harmonic-generation [20], optic index of refraction and strain [21] measurements.

Ever since the pioneering work of Glass [1] the relaxation dynamics of SBN61-type compounds has attracted great interest. However, the observed large dispersion and extreme sensitivity to an external electric field has not yet

[a] On leave from Institute of Physics, University of Silesia, 40–007 Katowice, Poland
[b] e-mail: wolfgang@kleemann.uni-duisburg.de

been explained in a satisfactory way. Smolenskii's original relaxor concept [22] has been used, which explains the diffuse nature of the ferroelectric phase transition within a broad "*Curie* range" by compositional fluctuations due to structural disorder of the solid solution. This picture has, however, largely been modified also in conventional relaxor physics since more than ten years. Today primarily either random-bond "glassy" [23] or random-field (RF) models [24] of microscopically homogeneous, albeit disordered systems are considered. For cubic relaxor systems like $PbMg_{1/3}Nb_{2/3}O_3$ (PMN) a spherical random-bond random-field model [25] seems to be capable of explaining many of the properties observed. In the present paper we suggest random bonds to be irrelevant in the case of the highly anisotropic uniaxial SBN system. We rather propose SBN to belong to the RF Ising model (RFIM) universality class, a rare case among structural phase transitions.

From a theoretical point of view this appears quite attractive, since in case of sufficiently weak RFs a sharp phase transition may occur in an Ising system, whereas it is definitely smeared in more isotropic pseudospin symmetry [26]. It is, hence, worthwhile checking the sharpness of the phase transition and the very occurrence of long-range order in the low temperature phase of SBN61 and its doped derivatives. Nearly all of the previous work was done on pure SBN albeit with various Sr/Ba ratios. The only preliminary report [17] on the dielectric response of SBN:Ce does not comprise frequency and field dependencies. These are of special interest, since doping with Ce^{3+} is expected to enhance both the charge and the structural disorder. Hence, it might be anticipated that both RFs and competing random bonds [23] will eventually favor the appearance of a glassy low temperature state at high enough x(Ce).

The present paper reports on results of systematic temperature and frequency dependent measurements of dielectric susceptibility of pure and Ce^{3+} doped SBN61 system both in poled and unpoled states. The Ce^{3+} ions ($r = 1.034$ Å) are known to substitute the ferroelectrically "silent" alkaline earth ions Sr^{2+} [27]. Owing to their different charge they are, hence, expected to primarily increase the average amplitude of the RFs and, in consequence, to diminish the average size of the nanodomains [26]. It is expected that macroscopic sample, which contains a myriad of independently exponentially relaxing regions forms a polydispersive response, which may be analyzed within the framework of the "dynamically correlated domains" (DCD) concept [28].

2 Experimental procedure

Pure SBN61 and Ce-doped crystals were grown by the Czochralski technique. Large and clear optical-quality single crystal bars have been obtained. Platelet samples of about $5 \times 5 \times 1$ mm^3 were cut with the polar c-axis normal to the planes of the plates. After polishing to optical quality copper electrodes extending to the crystal edges were vacuum evaporated on the major faces. In order to prevent the electrodes to be oxidized the copper was covered with a silver paste layer. This proved to be sufficient, since only moderate temperatures ($T < 500$ K) were used and the sample chamber was filled with He contact gas. The complex susceptibility, $\chi = \chi' - i\chi''$, was measured with a Hewlett-Packard 4192A impedance analyzer at temperatures $300 < T < 470$ K and frequencies $10^2 < f < 10^6$ Hz. The dielectric measurements were performed in the unpoled and poled states of the sample. The data were collected under isothermal conditions while starting from room temperature and reaching every point upon heating at a rate of 1 K/min. Before each run the sample was refreshed at 470 K for about 15 min. and then cooled down. For poling a dc field in the order of 3.5 kV/cm was maintained during cooling [16,29].

3 Results and discussion

The temperature dependencies of χ'_{33} (Fig. 1) show rounded peaks, which are shifted towards lower temperatures by doping with Ce^{3+} [17]. Simultaneously the peaks decrease and become broader in comparison with those of pure SBN61. Surprisingly, the temperature $T_m(\chi'_{33})$ of the maximum of χ'_{33} depends only weakly on the frequency at low f, but much stronger at high f. In parallel, the peak value of χ'_{33} strongly drops with increasing frequency. At $f = 10$ MHz the curve becomes essentially flat in comparison with the 100 Hz one. This behaviour differs strongly from that of the classic PMN relaxor [30]. Poling generally enhances the χ'_{33} peaks (by about 10% at $f = 100$ Hz), makes them sharper (especially in the low frequency limit) and shifts them towards lower temperatures in comparison with the unpoled case (Fig. 2). The difference between poled and unpoled state is small at low frequencies, but increases remarkably in the high frequency limit. As a result the poled sample shows a weaker frequency dependence of $T_m(\chi'_{33})$ than the unpoled one. This is shown in the inset of Figure 2, where the $T_m(\chi'_{33})$ *vs.* f data of the unpoled sample have been fitted to the well known Vogel-Fulcher relationship [31]:

$$f = f_0 \exp\left(-\frac{T_0}{T_m - T_f}\right) \quad (1)$$

with fitting parameters T_0, T_f and f_0 as listed in Table 1.

It is seen that the fits are excellent at not too low a temperature ($T > T_c \approx 360$ and 340 K for $x = 0$ and 0.0066, respectively). Here T_c is defined as the temperature below which stationarity of the susceptibility peak is encountered. Obviously both compounds bear glass-like properties only in the paraelectric regime, *i.e.* above T_c. Consequently, the extrapolated freezing temperature, T_f, is definitely lower than $T_c \approx T_m$ (10^2 Hz). This seems to indicate that the glassy freezing is never reached on cooling, but is replaced by quasi-critical behaviour due to the ferroelectric instability in the vicinity of T_c. We consider this to be typical of the Ising-type relaxor behaviour as conjectured above. It should be noticed, however, that criticality which is expected to be of the RFIM

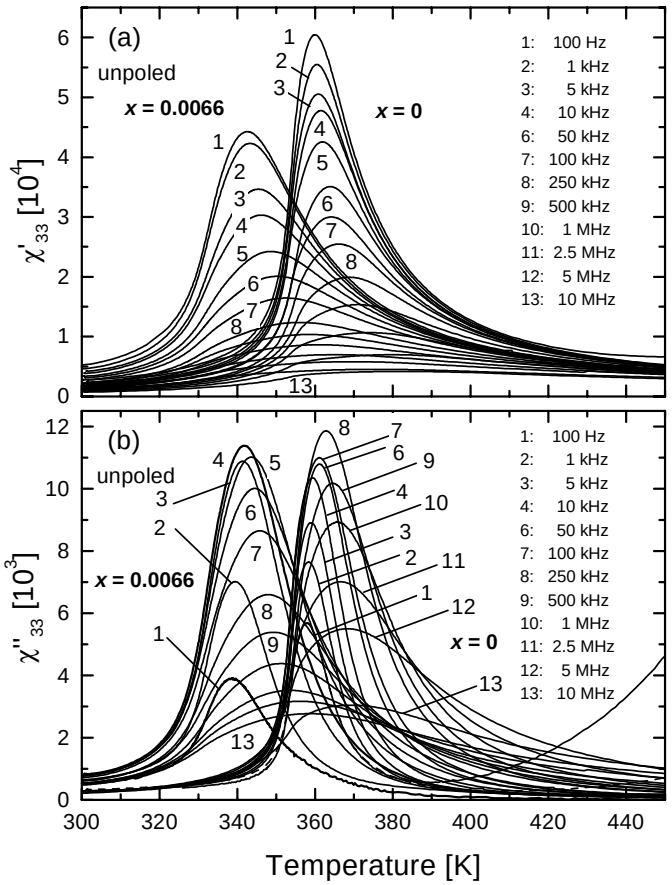

Fig. 1. Temperature dependencies of the susceptibility components χ'_{33} and χ''_{33} measured on unpoled SBN61:Ce with $x(\mathrm{Ce}) = 0$ and 0.0066 for frequencies $10^2 \leq f \leq 10^7$ Hz and temperatures $300 \leq T \leq 450$ K. A conductivity tail of χ''_{33} is observed at $T > 400$ K for $x = 0$ and $f = 10^2$ Hz.

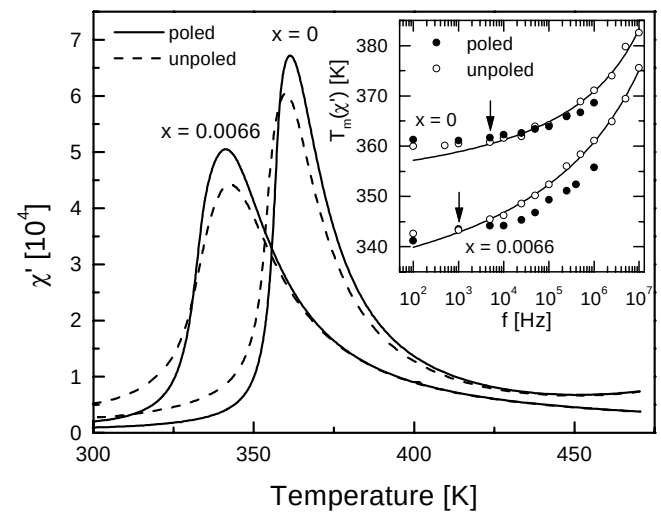

Fig. 2. Comparison of the poled and unpoled susceptibility χ'_{33} measured as a function of T at $f = 10^2$ Hz for $x(\mathrm{Ce}) = 0$ and 0.0066. The inset shows the frequency dependencies of the peak temperature T_m in comparison with best-fitted Vogel-Fulcher law [31], equation (1).

Table 1. Best-fit parameters of the $T_\mathrm{m}(\chi'_{33})$ *vs.* f data shown in Figure 2 (inset) to the Vogel-Fulcher law, equation (1).

x	T_f [K]	T_0 [K]	f_0 [Hz]
0.0	347 ± 3	160 ± 40	$(8 \pm 6) \times 10^8$
0.0066	320 ± 2	368 ± 49	$(8 \pm 5) \times 10^9$

type is not accessible by our ac susceptibility measurements. Severe rounding of the χ'_{33} peaks is encountered at $|T/T_\mathrm{c} - 1| < 10^{-2}$ even at the lowest frequency available, $f = 10^2$ Hz. That is why we preferred to determine critical exponents by using quasistatic measurements of the linear birefringence, which yields much clearer evidence of the conjectured RFIM universality class [32].

The parameter $T_0 = E_\mathrm{a}/k_\mathrm{B}$ is a measure of the average activation energy, E_a, where k_B is Boltzmann's constant. It increases by a factor of two when doping SBN61 with Ce^{3+}. This underlines that the dopant roughens the free energy landscape of the relaxing system by enhancement of the charge disorder. The values of the attempt frequency, $f_0 \approx 10^8$ Hz, are way below the soft-mode frequency, which is in the order 10^{10}–10^{11} Hz. RF-correlated polar clusters beyond the atomic scale are suggested to be at the origin of this anomaly. Our analysis of the frequency dependence of $T_\mathrm{m}(\chi'_{33})$ seems to show that, in contrast with the cubic relaxor PMN, global symmetry breaking takes place at T_c in SBN61. Thus a structural phase transition is encountered, which is preceded by relaxor-like precursor behaviour in the paraelectric temperature range.

Interestingly, some of the mesoscopic domain structure of the relaxor regime seems to survive also in the ferroelectric regime. This is evident from poling experiments, which yield notable changes of χ'_{33} in the room temperature limit. Generally, after poling the room temperature values of χ'_{33} are smaller (*e.g.* by a factor of 3 for SBN61:Ce at $f = 100$ Hz). Obviously the poling favors the single domain state and thus eliminates most of the domain wall contributions to the dielectric response. Very probably the rich ferroelectric domain structure, which is known to occur in the absence of an aligning field [33], is stabilized and controlled by the fluctuations of the quenched RFs. This became evident also from recent atomic force microscopical studies on SBN61 [34].

Figure 3 shows the dielectric spectra of the doped SBN61 sample both in unpoled and poled states. The temperature ranges $T < T_\mathrm{c}$ and $T > T_\mathrm{c}$ are distinguished by open and solid symbols, respectively. As is seen from Figure 3a, the dispersion of χ'_{33} in the unpoled sample gradually increases when increasing the temperature. At $T > 320$ K two regions with different slopes are distinguished. The flat slope governing the low-f range ($f < 10^4$ Hz) is tentatively ascribed to walls referring to macroscopic domains, whereas the steep one at higher frequencies ($f > 10^5$ Hz) probably refers to polar regions of nanoscale size. The macroscopic domain contribution is visibly reduced in the poled sample (Fig. 3c), where the room temperature spectrum becomes practically flat

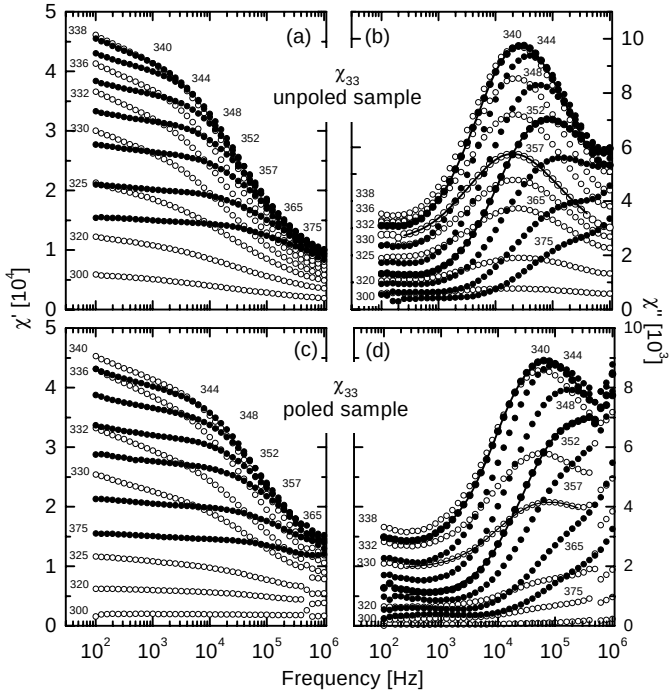

Fig. 3. Poled and unpoled dielectric spectra $\chi'_{33}(f)$ and $\chi''_{33}(f)$ of SBN61:Ce with $x(\mathrm{Ce}) = 0.0066$ at various constant temperatures $300 \leq T \leq 375$ K. Solid lines refer to selected fits to Chamberlin's expression [28], equation (2).

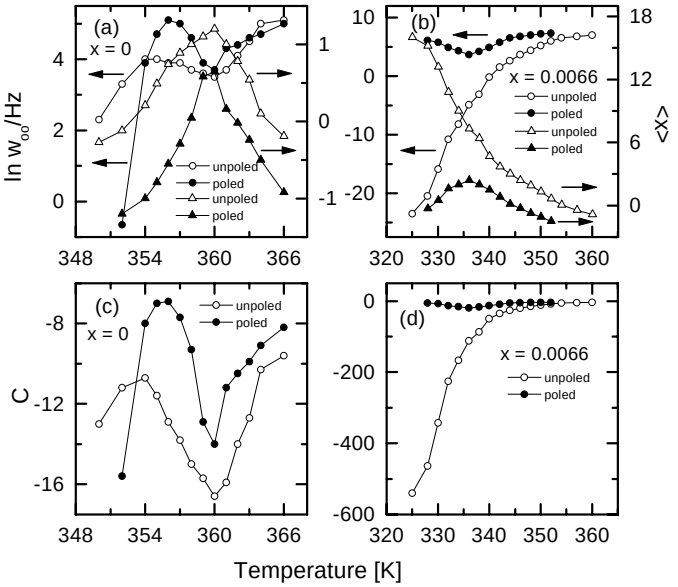

Fig. 4. Fit parameters according to equation (2) as obtained from the dielectric spectra $\chi''_{33}(f)$ of SBN61:Ce with $x(\mathrm{Ce}) = 0$ and 0.0066 (Fig. 3).

with low absolute values of χ'_{33}. However, this ferroelectric single domain state becomes unstable upon heating and approaching T_c. The finite slope encountered in the undoped sample reappears at $T \approx 340$ K. Obviously the thermodynamic fluctuations accompanying the critical region compete, again, with those of the quenched RFs and give rise to polydispersivity.

It is remarkable that dielectric losses, χ''_{33}, peak at nearly constant frequency below T_c, but move towards higher frequencies above T_c (Figs. 3b and d). Obviously a frozen domain structure with constant intermediate relaxation frequencies characterizes the ferroelectric state below the transition temperature, whereas in the relaxor regime above T_c the typical freezing scenario of temperature dependent distribution of domain sizes takes place. The losses are well described by Chamberlin's DCD concept of heterogeneous polydispersivity [28], where

$$\chi''(f) = \Phi_0 \int_0^\infty \mathrm{d}x[xn(x)] \frac{2\pi f/w(x)}{1 + [2\pi f/w(x)]^2} \qquad (2)$$

with the relaxation rate $w(x) = w_\infty \exp(-C/x)$ and a Gaussian domain size distribution $n(x) \propto \exp[-(x - \langle x \rangle)^2]$. Equation (2) is essentially a sum over an infinite number of non-interacting domains of size x, which exhibit Debye-type relaxation with size dependent relaxation rates, $w(x)$. The sign of the correlation coefficient C discriminates between activated ($C > 0$) and non-activated processes ($C < 0$), which occur in early and late stages of the relaxation process and roughly refer to power law (Curie-von Schweidler) or stretched exponential (Kohlrausch-Williams-Watts) temporal dependencies, respectively. A Gaussian distribution as found in the present case is typical of systems, which are close to ergodicity. It should be noticed that for strongly non-ergodic glass-like systems a percolation-type Poisson distribution would be expected.

Equation (2) contains four adjustable parameters: Φ_0 accommodates the magnitude of response, w_∞ governs the response time of large clusters, the correlation coefficient C and the normalized average domain size, $\langle x \rangle$, determine the shape and the width of the distribution function. Two of these parameters, *viz.* w_∞ and $\langle x \rangle$, are microscopic and characterize the local polar clusters.

Figure 4 shows the temperature dependencies of $\ln w_\infty$, $\langle x \rangle$, (Figs. 4a and 4b) and C (Figs. 4c and 4d) for both investigated compounds in their unpoled and poled states, respectively. Let us first discuss the behaviour of the parameters in the relaxor regimes, *i.e.* at $T > 360$ and 340 K for $x = 0$ and 0.0066, respectively. It is seen that $\ln w_\infty$ decreases upon cooling towards T_c in all cases, the variation being largest for the unpoled $x = 0.0066$ sample. This complies with the extreme degree of quenched disorder in the latter sample. Next, the values of $\langle x \rangle$ unanimously increase when approaching T_c from above. This is in agreement with the idea that the nanodomains will grow upon approaching the critical region as a result of the increasing thermal, but quenched spatial RF fluctuations. In some cases negative values of $\langle x \rangle$ are encountered (Fig. 4a), which denote that truncated Gaussian distributions are involved. Finally, the correlation factors C turn out to be negative in all cases considered. This is the signature of non-activated relaxation of the Kohlrausch-Williams-Watts-type, which is typical of the asymptotic temporal regime, $t \to \infty$, of glasses [28]. It is seen that

$|C|$ appreciably rises in the region of critical fluctuations as $T \to T_c^+$, most significantly, as expected, for the unpoled sample.

It should be stressed that poling definitely changes the parameters also above T_c *i.e.* in the paraelectric phase. This means that the dynamic multidomain state evolving in this region strongly depends on the initial state achieved below T_c. Very probably field cooling cancels much of the RF activity of a given sample by aligning defects similarly as has been observed in the doped relaxor system $K_{1-x}Li_xTaO_3$ [35]. Hence, the signatures of polydispersivity, in particular the $|C|$ values, decrease by poling prior to heating to above T_c. In addition, Vogel-Fulcher behaviour becomes less significant as evidenced by flat T_m *vs.* f curves in the poled state (Fig. 2, inset). It will be interesting to study this tendency on SBN61 doped with variant amounts of Ce^{3+} or other dopants.

Surprisingly, below T_c the behaviour of nearly all parameters shows drastic changes. In Figure 4 we observe sharp inversions of the temperature derivatives of $\ln w_\infty$, $\langle x \rangle$ and $C(x = 0)$. This is a clear hint at the crossover of the systems from relaxor to ferroelectric behaviour. However, the extreme rise of $|C|$ up to 600 observed in the case of the $x = 0.0066$ sample (Fig. 4d) appears unphysical and advises us to be careful with the interpretation of *all* results obtained at $T < T_c$. It should be recalled that all fits have been done with merely one set of parameters. This assumption does probably not hold in the ferroelectric regime, where both macroscopic polar domains and RF controlled mesoscopic domains are likely to coexist [34]. Hence, two distribution functions of domain sizes with different relaxation parameters presumably apply to this regime. This is indicated by the double slope in the real part of the susceptibility spectra (Figs. 3a and 3c) and by second peaks of χ''_{33}, which evolve at low frequencies, $f < 100$ Hz (Figs. 3b and 3d). Since data from this region are lacking at present, the final discussion of the polydispersivity applicable to temperatures below T_c must be postponed.

4 Conclusion

The assessment of our susceptibility data obtained on SBN61:Ce has shown that relaxor properties prevail in the precursor regime at $T > T_c$, whereas ferroelectricity is encountered for $T < T_c$. As usual, the relaxor regime is characterized by a diffuse and frequency dependent permittivity peak with a relaxation spectrum being much broader than Debye-type. Signatures of ferroelectric behaviour are the rapid drop of χ'_{33} below T_c (Figs. 1 and 2), the occurrence of macroscopic polar domains [33,34], and the comparatively low coercive fields [29]. From a Vogel-Fulcher analysis it seems to follow that the hypothetical freezing temperature T_f in SBN61-type relaxors falls below the actual Curie temperature, T_c. This contrasts with the experience on PMN-type perovskite relaxors, where glassy freezing takes place at much higher temperatures than the hypothetical Curie temperature [23]. Since these systems are known to exhibit competing ferro- and antiferroelectric coupling [23], a spin glass description seems adequate in a first approximation.

In the case of the open tungsten bronze structure of SBN61 this question is far from being settled. Based on our present experience we suggest that the random field mechanism is the prevailing one in this case. Very probably only the precursor regime displays typical relaxor properties, which are due to spatial fluctuations of the RFs. They are at the origin of the extreme critical slowing down, which may eventually smear the ferroelectric phase transition. Nevertheless, upon cooling to below T_c considerable growth of the nanodomains up to macroscopic size [33,34] seems to take place owing to long-range dipolar interaction. This is at variance with the well-known RF-cooled nanodomain structures of dilute antiferromagnetic Ising systems, which virtually do not coarsen upon annealing below T_c [23]. Clearly, the growth of macroscopic ferroelectric domains under counteraction of the RFs merits further attention. In particular, it will be interesting to study the relaxation kinetics of domains in SBN61 in the vicinity of T_c in future investigations.

Work supported by Deutsche Forschungsgemeinschaft within the framework of the Schwerpunktprogramm "Strukturgradienten in Kristallen" and Sonderforschungsbereich 225.

References

1. A.M. Glass, J. Appl. Phys. **40**, 4699 (1969).
2. R.R. Neurgaonkar, M.H. Kalisher, T.C. Lim, E.J. Staples, K.L. Keester, Mater. Res. Bull. **15**, 1235 (1980).
3. K. Tada, T. Murai, M. Aoki, K. Muto, K. Awazu, Jpn J. Appl. Phys. **11**, 1622 (1972).
4. R. R. Neurgaonkar, W.K. Cory, J.R. Oliver, Ferroelectrics **51**, 3 (1983).
5. E.L. Venturini, E.G. Spencer, A.A. Ballman, J. Appl. Phys. **40**, 1622 (1969).
6. B. Fisher, M. Cronin-Golomb, J.O. White, A. Yariv, R.R. Neurgaonkar, Appl. Phys. Lett. **40**, 863 (1982).
7. G. Salamon, M.J. Miller, W.W. Clark III, G.L. Wood, E.J. Sharp, Opt. Commun. **59**, 417 (1986).
8. R.R. Neurgaonkar, W.K. Cory, J. Opt. Soc. Am. B **3**, 274 (1986).
9. R.R. Neurgaonkar, W.K. Cory, J.R. Oliver, M.D. Ewbank, W.F. Hall, Opt. Eng. **26**, 392 (1987).
10. S.C. Abrahams, P.B. Jamieson, J.L. Bernstein, J. Chem. Phys. **54**, 2355 (1971).
11. F. Micheron, C. Mayeux, J.C. Trotier, Appl. Opt. **13**, 913 (1974).
12. J.R. Oliver, R.R. Neurgaonkar, L.E. Cross, J. Appl. Phys. **64**, 37 (1988).
13. Yu.C. Kuzminov, *Segnetoelektritcheskie kristally dla upravlenia lasernym izutcheniem* (Moskwa, Nauka 1982), p. 102.
14. M.E. Lines, A.M. Glass, *Principles and Application of Ferroelectrics and Related Materials* (Clarendon Press, Oxford 1979), p. 255.
15. L.A. Shuvalov, J. Phys. Soc. Jpn **28** (Suppl.), 38 (1970).

16. T. Volk, Th. Woike, U. Dörfler, R. Pankrath, L. Ivleva, M. Wöhlecke, Ferroelectrics **203**, 457 (1997).
17. N. Wittler, G. Greten, S. Kapphan, R. Pankrath, J. Seglins, Phys. Stat. Solidi (b) **189**, K37 (1995).
18. J.J. DeYoreo, R.O. Pohl, G. Burns, Phys. Rev. B **32**, 5780 (1985).
19. G. Burns, F.H. Dacol, Solid State Commun. **58**, 567 (1986).
20. T. Heinz, G. Burns, N. Halas, Bull. Am. Phys. Soc. **31**, 603 (1986).
21. A.S. Bhalla, R. Guo, L.E. Cross, G. Burns, F.H. Dacol, R.R. Neurgaonkar, Phys. Rev. B **36**, 2030 (1987).
22. G.A. Smolenskii, J. Phys. Soc. Jpn **28**, 26 (1970); L.E. Cross, Ferroelectrics **76**, 241 (1987); *ibidem* **151**, 305 (1994).
23. I.-W. Chen, P. Li, Y. Wang, J. Phys. Chem. Solids **57**, 1525 (1996); I.-W. Chen, J. Phys. Chem. Solids **61**, (2000).
24. V. Westphal, W. Kleemann, M. D. Glinchuk, Phys. Rev. Lett. **68**, 847 (1992); W. Kleemann, Int. J. Mod. Phys. B **7**, 2469 (1993).
25. R. Blinc, J. Dolinsek, A. Gregorovic, B. Zalar, C. Filipic, Z. Kutnjak, A. Levstik, R. Pirc, Phys. Rev. Lett. **83**, 424 (1999).
26. Y. Imry, S.K. Ma, Phys. Rev. Lett. **35**, 1399 (1975).
27. Th. Woike, G. Weckwerth, H. Palme, R. Pankrath, Solid State Commun. **102**, 743 (1997).
28. R.V. Chamberlin, Phys. Rev. B **48**, 15638 (1993); R.V. Chamberlin, Europhys. Lett. **33**, 545 (1996); R.V. Chamberlin, Phase Transitions **65**, 169 (1998).
29. Th. Woike, T. Volk, U. Dörfler, R. Pankrath, L. Ivleva, M. Wöhlecke, Ferroelectrics Lett. **23**, 127 (1998).
30. D. Viehland, M. Wuttig, L.E. Cross, Ferroelectrics **120**, 71 (1991).
31. H. Vogel, Phys. Z. **22**, 645 (1921); G.S. Fulcher, J. Am. Ceram. Soc. **8**, 339 (1925).
32. P. Lehnen, W. Kleemann, Th. Woike and R. Pankrath, Eur. Phys. J. B **14**, 633 (2000).
33. L.A. Bursill, P.J. Lin, Philos. Mag. B **54**, 157 (1986).
34. Y.G. Wang, W. Kleemann, Th. Woike, R. Pankrath, Phys. Rev. B **61**, 3333 (2000).
35. H. Schremmer, W. Kleemann, D. Rytz, Phys. Rev. Lett. **62**, 1896 (1989).